
Superimposed Display of Coronary Artery on Gated Myocardial Perfusion Scintigraphy

Yoshihiro Nishimura, MSc^{1,2}; Kazuki Fukuchi, MD¹; Tetsuro Katafuchi, PhD¹; Masayoshi Sagou, BSc¹; Hisashi Oka, BSc¹; Yoshio Ishida, MD¹; and Kenya Murase, PhD²

¹Department of Radiology, National Cardiovascular Center, Suita, Osaka, Japan; and ²Division of Medical Technology and Science, Department of Medical Physics and Engineering, Course of Health Science, Graduate School of Medicine, Osaka University, Suita, Osaka, Japan

Fusion of images of vascular anatomy and of myocardial perfusion images might be helpful for understanding the relationship between ischemia and the responsible vessels. The aim of this study was to develop a simple means of superimposing the images obtained from coronary angiography and gated myocardial perfusion SPECT. **Methods:** Right and left oblique views from conventional coronary angiography and left ventriculography (LVG) were stored as $512 \times 512 \times 8$ -bit digital datasets and combined. We reconstructed images from routine gated myocardial perfusion imaging (MPI) by using ^{99m}Tc-tetrofosmin to match the oblique positions between the image from MPI and combined angiographic images. We then generated a 3-dimensional (3D) surface map by using the quantitative gated SPECT (QGS)/quantitative perfusion SPECT (QPS) program. Both the combined angiographic images and the 3D surface map were rescaled and unified by registering the internal landmarks between the 2 images. After subtraction of the LVG image, the coronary angiogram and the 3D surface map were fused into 1 image. All processes were performed with the QGS/QPS program and commercially available graphic software. We applied this method to datasets from a cardiac phantom and from several patients with coronary artery disease. **Results:** In the phantom study, our technique could obtain a 3D surface map in which the oblique angle was identified as that of radiography and could realize image registration and superimposition of radiography on scintigraphy. The preliminary results from the patients indicated that the markedly stenotic vessels showed good coincidence with the regional myocardial perfusion abnormalities on the unified images. In addition, these images could show the relationship between the coronary artery and regional wall motion in the gated mode. **Conclusion:** We developed a simple method of superimposing the image of the coronary artery tree on images from gated MPI. The technique yielded useful information about myocardial perfusion and function as well as the supplying coronary artery.

Key Words: coronary angiography; myocardial perfusion; image fusion

J Nucl Med 2004; 45:1444–1449

Received Dec. 18, 2003; revision accepted Mar. 2, 2004.

For correspondence or reprints contact: Kazuki Fukuchi, MD, Department of Radiology, National Cardiovascular Center, Fujishiro-dai 5-7-1, Suita, Osaka 565-8565, Japan.

E-mail: kfukuchi@hsp.ncvc.go.jp

Patients with coronary artery disease are usually assessed by coronary angiography to determine epicardial coronary artery stenosis (1–3). On the other hand, regional myocardial perfusion is frequently evaluated by myocardial SPECT (4,5). A physician then typically reviews images generated from these modalities by subjective, visual observation. Although the segments in images from myocardial perfusion imaging (MPI) are arbitrarily assigned to 3 major coronary artery systems, the standard myocardial distribution territories of the coronary tree correspond only in 50%–60% of patients (6). Moreover, the mental integration of coronary angiography and MPI cannot accurately assign any specific myocardial perfusion defect to the responsible vessels. Therefore, image registration between coronary vascular anatomy and regional myocardial perfusion should improve the diagnosis of culprit coronary lesions that cause myocardial ischemia and provide useful information for making decisions regarding coronary revascularization (7–9). Some studies have produced 3-dimensional (3D) fusion images from coronary angiography and MPI, but the procedure is time-consuming and accurate evaluation requires detailed knowledge of the process (10–14).

The aim of this study was to develop a simple and practical means of generating unified images from coronary angiography and gated MPI. We used the quantitative gated SPECT (QGS)/quantitative perfusion SPECT (QPS) program that is routinely used in nuclear cardiology examinations, as it can provide 3D surface myocardial perfusion maps that suit image registration (15,16).

MATERIALS AND METHODS

Figure 1 shows a schematic outline of the image registration procedure. Biplane digital angiography, including coronary angiography and left ventriculography (LVG), conventionally proceeded from the left anterior oblique (LAO) angle of 60° (LAO-60°) and the right anterior oblique (RAO) angle of 30° (RAO-30°). The coronary angiogram was superimposed on the LVG image to generate combined angiographic images in each oblique view. LVG and coronary angiography were simply registered by translation, because both were taken from the same views in the same manner.

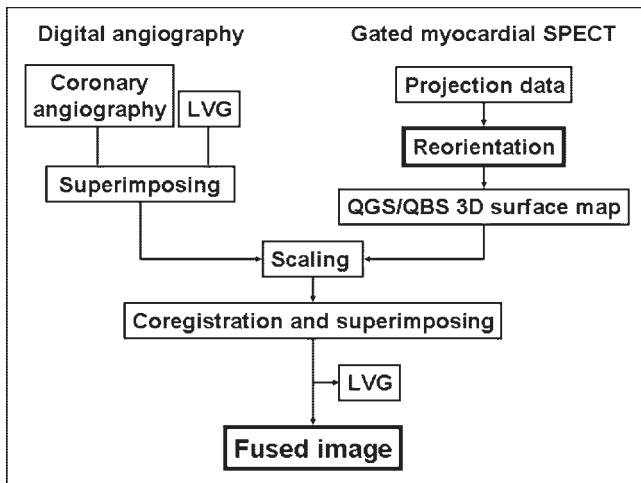


FIGURE 1. Basic flow chart of image fusion between coronary angiography and gated MPI.

The patients underwent gated MPI on a different day. The QGS/QPS program includes a set of frequently used 3D surface views, including RAO and LAO, and these views can be easily selected (15,16). However, these views could not be directly superimposed on coronary angiograms because the oblique axis of reorientation of the image from MPI corresponds to the natural axes of the heart. To superimpose a coronary angiogram on a 3D surface map, both images should have the same oblique angle based on the body axis of the patient. Therefore, the long axis of the left ventricle for reorientation was set to correspond to the coronary angiogram (Fig. 2).

After reorientation and reconstruction, the QGS/QPS program generated a 3D surface map. We selected a 3D surface map that displayed the endocardial surface as a solid volume and the epicardial wall as a wire-frame surface. For registration of the combined angiographic images and the 3D surface map, both images required scaling. If the length of the 3D surface map could be calibrated with a known phantom size, then the coronary angiographic data could be scaled to the size of the corresponding 3D surface map with a known scale factor. We registered the endocardial surface of the 3D surface map and the left ventricular contour of the combined angiographic images by minimizing the average distance between the 2 surfaces. After registration, the 3D surface display was changed to a colored map reflecting the relative count distribution. Subsequently, the LVG was eliminated from the combined angiographic images. Finally, the superimposed image was obtained by integrating the coronary angiogram with the 3D surface map from gated MPI.

The acquired coronary angiographic and LVG images were stored on CD-R with the audio-video-interleave file format of 512×512 matrix, 8 bits, and 256 density levels (17). The data for the 3D surface map were stored as a single cardiac cycle frame with the tagged information file format. Both datasets were transferred to a personal computer, and commercial image analysis software was used for image registration and superimposition (Adobe Photoshop 6.0; Adobe Systems).

Phantom Study

We investigated the feasibility of reoriented SPECT by using a phantom (model RH-2; Kyoto-Kagaku Hyohon) representing a

myocardium with 3 small subendocardial defects that corresponded to perfusion abnormalities and a left ventricle. The wall thickness was 10 mm, and the volume of the left ventricle was 172 mL. The myocardium was filled with ^{99m}Tc -pertechnetate-diluted water (18), and then the phantom was imaged by use of a biplane, multidirectional, digital angiographic system (DFP-2000A; Toshiba Co.) at RAO-30° and LAO-60°. The calibration cube and a flat calibration grid were filmed after imaging to calibrate the x-ray geometric settings. Thereafter, the SPECT images were acquired by use of a dual-headed angular rotating γ -camera system (VERTEX; ADAC Laboratories) equipped with a low-energy general-purpose collimator. The SPECT image acquisition parameters were as follows: 180° (30 steps; 6°/step), 64×64 matrix, and 20% main window centered at the photopeak energy of ^{99m}Tc (140 keV). The images were reconstructed by use of maximum-likelihood expectation maximization with Butterworth filtering (cutoff, 0.42–0.45 cycles/cm; order, 10).

The registration accuracy was estimated from the distances between the centers of the subendocardial defects on both the angiogram and the 3D surface map from scintigraphy after superimposition. The distances were calculated by a previously described method (19). Interobserver analysis was performed by 2 independent observers, and intraobserver analysis was done twice by the same observer.

Clinical Study

Conventional coronary angiography and LVG were performed by use of the same digital angiographic system as that used for the phantom study. Standard orthogonal biplane images were acquired at a frame rate of 15 frames per second. Coronary angiography was performed at various imaging angles, including the standard angles (LAO-60° and RAO-30°). The patients were injected with 592 MBq of ^{99m}Tc -tetrofosmin while at exercise or rest for gated MPI. SPECT images were acquired by use of the same γ -camera system and acquisition parameters as those applied in the phantom study. We used 8 individual electrocardiography (ECG)-gated frames per cardiac cycle (50 beats/step) during each projection.

To confirm the reliability of the QGS/QPS parameters when our reorientation method was applied to the clinical data, we randomly

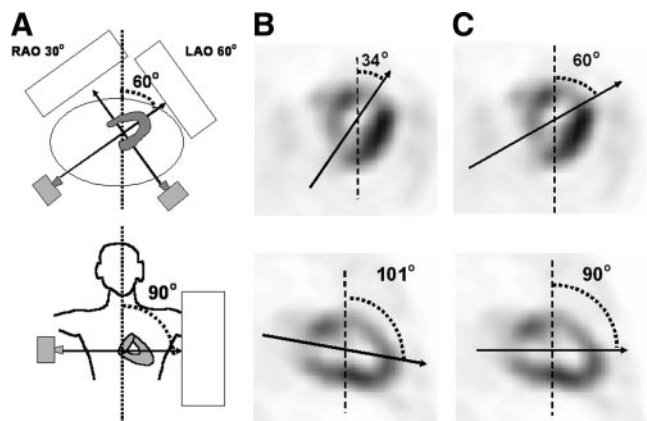


FIGURE 2. Principles of MPI reorientation. To obtain the same oblique angle as in biplane coronary angiography (A), we changed the conventional setting of the long axis of the left ventricle for reorientation (B) to a new setting for the long axis that was consistent with both LAO-60° and RAO-30° views (C).

chose 20 images from gated MPI and reconstructed their projection data by using both the original and the reorientation methods. The left ventricular volumes, ejection fractions, and extent of perfusion defects were calculated by use of the QGS/QPS program.

For superimposition of the coronary artery on images from MPI, we used data from several patients who were referred to our hospital for cardiac angiography and MPI. All patients underwent coronary angiography and LVG within 2 wk of gated MPI. ECG was simultaneously recorded during coronary angiography, and the coronary angiographic images of 1 cardiac cycle were divided into 8 groups in the manner used for 8-frame gated MPI. The 8 groups of coronary angiographic images were successively superimposed onto the corresponding 8 frames of the 3D surface map from gated MPI. This procedure generated a cine-like image of the fused 3D surface map.

Statistical Analysis

Registration accuracy and reproducibility were compared by use of the Student *t* test. Linear regression analysis was performed to calculate the linear dependency measurements of the left ventricular volumes, ejection fractions, and extent of perfusion defects by use of both the original and the reorientation methods of reconstruction in the QGS/QPS program. Significance was established when the probability values were less than 0.05.

RESULTS

Phantom Study

Figure 3 compares the conventional QGS/QPS 3D surface maps of the cardiac phantom and those after reorientation during SPECT reconstruction. The RAO and LAO views of the conventional 3D surface maps did not contain exact information about the oblique angle to the axis of the object. Therefore, the rotation and inclination of the 3D surface maps did not correspond to those of the radiographic images at LAO-60° and RAO-30°. On the other hand, the reoriented 3D surface maps of the cardiac phantom had the same view angles as the radiographic images. This result is attributed to the fact that the images were reoriented in a manner similar to that used for the radiographic images. Thus, the perfusion defects in the 3D surface maps could be superimposed on those in the radiographic images.

The distances (mean \pm SD) between the defect in the radiographic image and that in the 3D surface map after image registration ($n = 10$) were 2.36 ± 0.95 mm in the first trial by observer 1, 2.26 ± 0.87 mm by observer 2, and 2.45 ± 1.20 mm in the second trial by observer 1. There were no significant differences among these distances.

Clinical Study

For the gated MPI data from our 20 cases, edge detection by the QGS/QPS program was successful for all of the cases. Moreover, there was good agreement for the left ventricular end-diastolic ($y = 0.99x + 0.63$; $r = 1.00$; $P < 0.0001$) and end-systolic ($y = 1.00x + 0.03$; $r = 1.00$; $P < 0.0001$) volumes and ejection fractions ($y = 0.99x + 0.40$; $r = 0.99$; $P < 0.0001$) between the 2 methods in the QGS program. There was also a high linear correlation for the extent of perfusion defects in the QPS program ($y = 0.96x - 0.32$; $r = 0.99$; $P < 0.0001$). These results indicate that the functional parameters of gated MPI were equal for the original reconstruction method and the reorientation method.

The left coronary tree was superimposed on the 3D surface map from MPI by use of the data from our patients. In addition to the LAO-60° and RAO-30° images, we obtained fused images at the left posterior oblique (LPO) angle of 30° (LPO-30°) when the RAO-30° 3D surface map was rotated 180° and a mirror image of the left coronary arteriogram was created by the graphic software (Fig. 4). The septal and lateral views at RAO-30° and LPO-30° of the left coronary angiogram can distinguish whether a perfusion abnormality is located in the left descending coronary artery or the diagonal branch. The anterior view from LAO-60° is also useful for assessing the left circumflex artery and its corresponding perfusion territory. Superimposing the right coronary arteriogram on the 3D septal view can reveal information about regional perfusion in the distal part of the right coronary artery.

Coronary angiograms superimposed on exercise and rest images from MPI clarified the relationship between stenosis

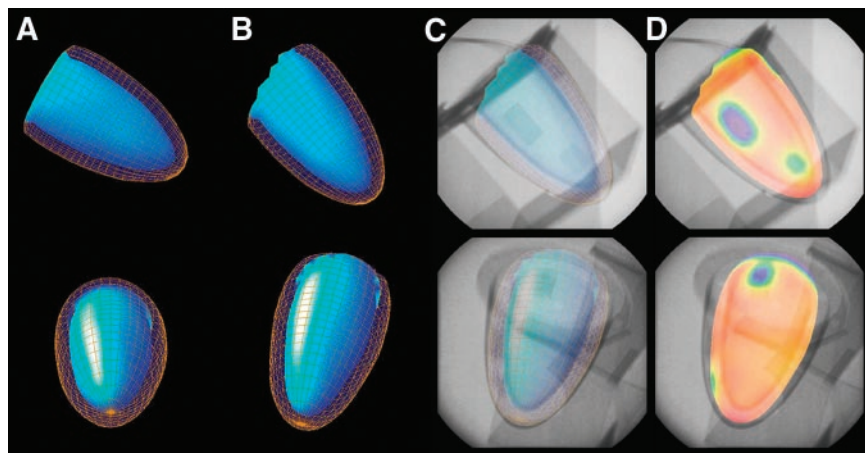


FIGURE 3. Results of phantom studies confirming the accuracy of reorienting the long axis of the left ventricle for image registration (top: RAO-30°; bottom: LAO-60°). (A and B) QGS 3D surface maps with inner and outer cardiac walls generated by the conventional method (A) and after reorientation (B). (C) Reoriented 3D surface maps were superimposed on radiographic images at RAO-30° and LAO-60° views. (D) Changing the surface display allowed the colored 3D map to reflect the relative count distribution with the fused radiographic image.

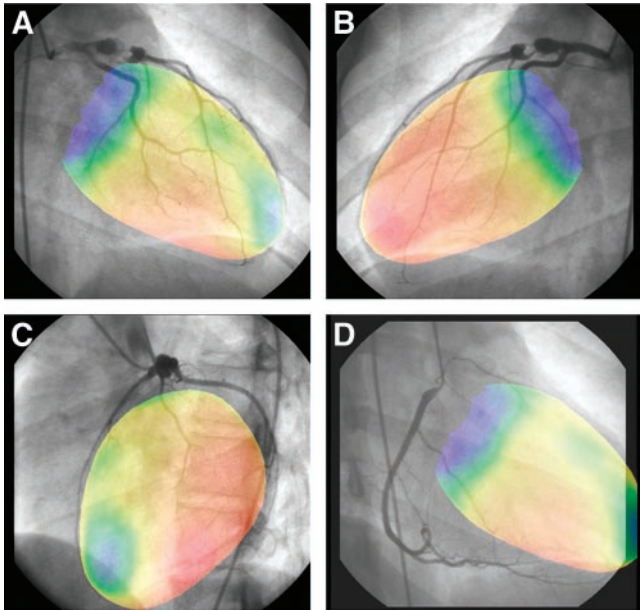


FIGURE 4. Superimposed displays of a coronary angiogram and an exercise 3D surface map obtained from a 15-y-old girl with Kawasaki disease. An aneurysmal dilatation with distal stenosis (90% narrowing) was located in the proximal portion of the left anterior descending artery on coronary angiography. MPI showed anterapical hypoperfusion during exercise. The perfusion abnormality was obviously distributed in the distal territory of the left descending coronary artery (A) and not in the diagonal branch territory (B). Meanwhile, the anterior LAO-60° view (C) and superimposition of the right coronary artery on the septal view of MPI (D) are also available with our technique.

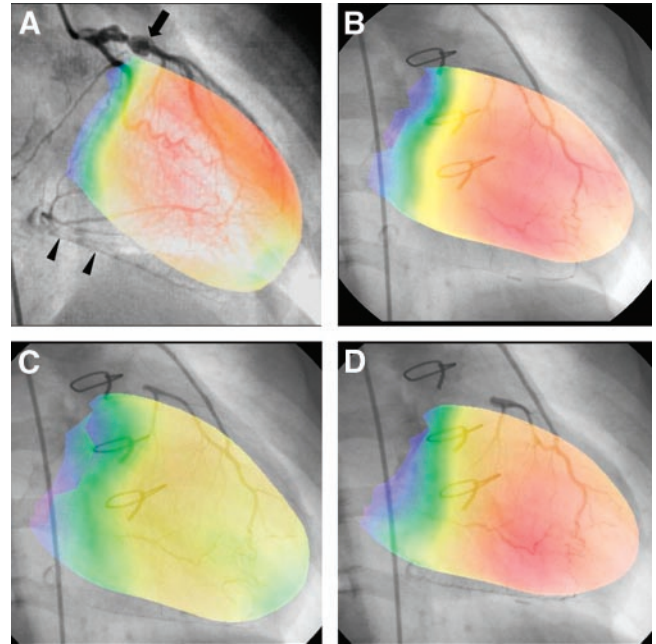


FIGURE 6. Superimposed displays of a coronary angiogram and an exercise 3D surface map obtained from an 11-y-old girl with Kawasaki disease. (A) The unified image depicts apical and inferior hypoperfusion and a coronary aneurysm (arrow) with distal stenosis in the left anterior descending artery. The right coronary artery (arrowheads) was filled by collateral vessels through the septal branch because the proximal portion of the right coronary artery was occluded. (B) After bypass surgery, the nongated unified image shows homogeneous left ventricular perfusion with patency of the left internal mammary artery bypass graft at exercise. (C and D) ECG-gated unified images at end-diastole (C) and end-systole (D) show normal regional wall motion and count increase in the left ventricular wall.

of the epicardial coronary artery and the extent of exercise-induced ischemia (Fig. 5). Furthermore, the gated unified images at end-diastole and end-systole could simultaneously express regional left ventricular function (wall motion and count increase during the cardiac cycle) and the corresponding coronary artery (Fig. 6). These images could

be displayed in cine mode like those in the standard QGS program.

DISCUSSION

The decision-making processes in medicine typically require integration of several types of information in a meaningful, reliable, and efficient manner. Coronary angiography is the accepted gold standard of cardiology for locating coronary artery stenosis. However, the hemodynamic significance of a coronary lesion cannot be assessed by coronary angiography alone (9). The degree of myocardial ischemia should be assessed by radionuclide imaging (20,21). For further therapeutic planning, including revascularization, mental integration between coronary angiography and MPI is needed, but the exact anatomic registration seems to be difficult. Thus, registration between both images is desirable. Here we describe a novel technique for superimposition of the coronary artery tree on gated images from MPI that is patient specific and that can display the relationship between coronary artery defects and perfusion abnormalities. This technique directly renders the impact of critical

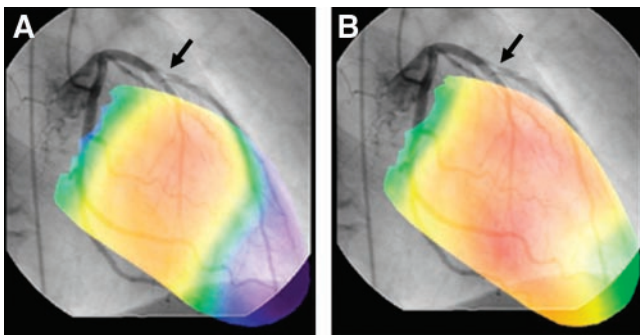


FIGURE 5. Superimposed displays of images from left coronary angiography and MPI at exercise (A) and rest (B) from a 57-y-old man with chest pain. The unified images show exercise-induced ischemia in the anteroapical myocardium in geometric correspondence with the diseased left anterior descending artery (arrow).

coronary artery stenosis on the peripheral vascular bed in a single image. Although it takes approximately 20 min of processing to realize the superimposed image, this method is simple and cost-effective because only the QGS/QPS program and personal computer-based graphic software are required.

The consistency of the oblique angle between both modalities is critical when one is processing the image registration between coronary angiography and gated MPI. Although the RAO and LAO views of the QGS/QPS 3D surface map are directly available from the program, these views are not similar to those of coronary angiography. We changed the angle of the oblique-axis reconstruction of MPI to match that of the coronary angiographic views. The phantom study revealed that the 3D surface map had the same oblique angle as the radiographic image when reoriented according to the theoretical alteration of the oblique axis. To apply this procedure to data from patients, a consistent view angle can be also realized between coronary angiography and gated MPI. Although an extra reconstruction must be added to routine image processing for this reorientation procedure, the oblique-axis angle can be simply and rapidly determined. We confirmed that the QGS/QPS parameters remained constant when the angle of the oblique-axis reconstruction of MPI was changed.

The QGS/QPS program can depict the left ventricular perfusion distribution with color coding to display the magnitude of the relative perfusion levels (15). This 3D color map may offer an accurate evaluation of the size and location of perfusion defects as well as a polar map or slice-by-slice displays. Because the QGS/QPS program is now regularly applied in most nuclear cardiology departments, the 3D surface map can be acquired without any expensive software—a significant advantage for practical use in the clinical setting.

We superimposed images from coronary angiography onto images from nongated and ECG-gated MPI—another advantage of our method. Previous studies that intended to register both images could not achieve cine displays of the fused data because the projection data from the coronary angiograms were too complex to use in a cine mode. We simply divided the cine data from coronary angiography into 8 frames per cardiac cycle, like the gated MPI data, and fused them. Thus, the gated and unified images revealed the degree of regional wall motion and count increase per cardiac cycle with the corresponding coronary artery. This information will be useful for decision making before coronary revascularization because information about regional myocardial contractility in addition to information about the quality and graftability of target vessels can be provided. Moreover, our unified images can depict both the patency of the vascular graft and the functional recovery after revascularization during follow-up.

The present study has some limitations. First, the views of the unified images were limited because conventional

LVG was performed in only 2 oblique views (i.e., RAO-30° and LAO-60°). The status of the right coronary artery cannot be appropriately assessed from these 2 views. To assess right coronary artery lesions in detail, we performed additional LVG at an oblique angle; this procedure helped in the observation of the right coronary tree. Our method could realize 2-dimensional registration between coronary angiography and gated MPI. Other investigators have superimposed a 3D coronary tree onto the epicardial contours of images from MPI (10–13). Although these methods are more sophisticated than ours, they did not work in clinical practice because the automated or semiautomated coronary tree traces could not provide accurate information about the vessel size or the severity of stenosis (10–13). In contrast, we superimposed an original image from coronary angiography on an image from gated MPI and transparently showed both. Although assessing an angiographic image of coronary arteries overlaid on a 3D surface map requires a specialist for interpretation, this image can include all of the information from the original coronary angiography image, for example, the degree of stenosis, the sizes of small vessels in the peripheral area, and the status of collateral flow. Thus, our technique allows an accurate evaluation of the perfusion territories of each coronary vessel and complements information about vessel anatomy that cardiologists need to know before deciding any further therapeutic strategies.

CONCLUSION

We developed a simple method for superimposing images from coronary angiography onto images from gated MPI. This procedure integrates anatomic and functional information to facilitate decision making by cardiologists and therefore can improve the management of patients with coronary disease.

ACKNOWLEDGMENT

A part of this study was financially supported by the Budget for Nuclear Research of the Ministry of Education, Culture, Sports, Science and Technology, based on the screening and counseling by the Atomic Energy Commission.

REFERENCES

1. Hale G, Dexter D, Jefferson K, Leatham A. Value of coronary arteriography in the investigation of ischaemic heart disease. *Br Heart J*. 1966;28:40–54.
2. Murphy ML, Galbraith JE, de Soyza N. The reliability of coronary angiogram interpretation: an angiographic-pathologic correlation with a comparison of radiographic views. *Am Heart J*. 1979;97:578–584.
3. Boucher RA, Myler RK, Clark DA, Stertzer SH. Coronary angiography and angioplasty. *Cathet Cardiovasc Diagn*. 1988;14:269–285.
4. Berman DS, Germano G, Shaw LJ. The role of nuclear cardiology in clinical decision making. *Semin Nucl Med*. 1999;29:280–297.
5. Verani MS. Thallium-201 single-photon emission computed tomography (SPECT) in the assessment of coronary artery disease. *Am J Cardiol*. 1992;70:3E–9E.

6. Kalbfleisch H, Hort W. Quantitative study on the size of coronary artery supplying areas postmortem. *Am Heart J*. 1977;94:183–188.
7. Mark DB, Lam LC, Lee KL, et al. Effects of coronary angioplasty, coronary bypass surgery, and medical therapy on employment in patients with coronary artery disease: a prospective comparison study. *Ann Intern Med*. 1994;120:111–117.
8. Pell JP, Denvir MA. Angioplasty, bypass surgery or medical treatment: how should we decide? *Heart*. 2002;88:451–452.
9. Chamuleau SA, van Eck-Smit BL, Meuwissen M, et al. Adequate patient selection for coronary revascularization: an overview of current methods used in daily clinical practice. *Int J Cardiovasc Imaging*. 2002;18:5–15.
10. Faber TL, Folks RD, Klein JL, et al. Myocardial area-at risk validates accuracy of automatic unification of coronary artery trees with SPECT [abstract]. *J Nucl Med*. 1999;40(suppl):78P.
11. Schindler TH, Magosaki N, Jeserich M, et al. Fusion imaging: combined visualization of 3D reconstructed coronary artery tree and 3D myocardial scintigraphic image in coronary artery disease. *Int J Card Imaging*. 1999;15:357–368.
12. Schindler TH, Magosaki N, Jeserich M, et al. 3D assessment of myocardial perfusion parameter combined with 3D reconstructed coronary artery tree from digital coronary angiograms. *Int J Card Imaging*. 2000;16:1–12.
13. Aguade S, Candell-Riera J, Faber TL, et al. Unified three-dimensional images of myocardial perfusion and coronary angiography. *Rev Esp Cardiol*. 2002;55:258–265.
14. Reiber JH. Where do I put my research money? *Int J Card Imaging*. 1999;15:369–370.
15. Germano G, Kiat H, Kavanagh PB, et al. Automatic quantification of ejection fraction from gated myocardial perfusion SPECT. *J Nucl Med*. 1995;36:2138–2147.
16. Germano G, Kavanagh PB, Berman DS. An automatic approach to the analysis, quantitation and review of perfusion and function from myocardial perfusion SPECT images. *Int J Card Imaging*. 1997;13:337–346.
17. Booth AG. Visualizing protein conformational changes on a personal computer: alpha carbon pseudo bonding as a constraint for interpolation in internal coordinate space. *J Mol Graph Model*. 2001;19:481–486.
18. Knesaurek K. A new dual-isotope convolution cross-talk correction method: a Tl-201/Tc-99m SPECT cardiac phantom study. *Med Phys*. 1994;21:1577–1583.
19. Eberl S, Kanno I, Fulton RR, et al. Automated interstudy image registration technique for SPECT and PET. *J Nucl Med*. 1996;37:137–145.
20. Legrand V, Mancini GB, Bates ER, Hodgson JM, Gross MD, Vogel RA. Comparative study of coronary flow reserve, coronary anatomy and results of radionuclide exercise tests in patients with coronary artery disease. *J Am Coll Cardiol*. 1986;8:1022–1032.
21. Miller DD, Donohue TJ, Younis LT, et al. Correlation of pharmacological ^{99m}Tc-sestamibi myocardial perfusion imaging with poststenotic coronary flow reserve in patients with angiographically intermediate coronary artery stenoses. *Circulation*. 1994;89:2150–2160.

